Applied Physics A (2022) 128:307
https://doi.org/10.1007/s00339-022-05367-6

Applied Physics A
Materials Science & Processing

Synthesis, characterization and cytotoxicity study of graphene/doped ZnO/SiO_2 nanocomposites

Mahshid Chireh[1] · Zahra Miri Karam[2] · Mahmoud Naseri[1] · Saeideh Jafarinejad-Farsangi[3] · Hamidreza Ghaedamini[4]

Received: 15 November 2021 / Accepted: 2 February 2022

Abstract
In the preset study, ZnO nanoparticles were synthesized by thermal treatment method and the ZnO/SiO_2 and ZnO/SiO2/RGO nanocomposites were obtained by polymerization method. The degree of crystallinity, microstructure and phase composition were investigated by using different characterization techniques, i.e., X-ray diffraction, field emission scanning electron microscope, transform infrared spectroscopy and Raman spectroscopy, respectively. The compositions of the samples were determined by Energy dispersive X-ray analysis at room temperature. The surface areas of samples were obtained from nitrogen gas adsorption–desorption isotherms by Brunauer–Emmett–Teller analysis at 77 K.
In addition, viability of breast tumor cells and normal 3T3-fibroblasts after exposure to RGO, of ZnO/SiO_2 and ZnO/SiO2/RGO were evaluated using MTT assay. RGO had no toxicity and almost all breast tumor cells and fibroblasts were viable after exposure to RGO. Furthermore, the toxic effect of ZnO/SiO_2/RGO and of ZnO/SiO_2 was more in breast tumor cells compared to normal 3T3 fibroblasts. However of ZnO/SiO_2 had a mild effect compared with ZnO/SiO_2/RGO.

Keywords Thermal treatment method · ZnO/SiO_2/RGO · Nanocomposite · MTT assay · Tumor cell

1 Introduction

An increasing deal of research indicated that certain kinds of metal oxide nanoparticles can selectively kill cancer cells and at the same time, be of low toxicity to their normal counterparts [1]. Former studies demonstrated that ZnO nanoparticles are toxic to some degree in a large number of organisms such as protozoa, bacteria, microalgae, zebrafish, yeast, and mice [2]. Therefore, ZnO nanoparticles need to be tailored with improved selectivity and anticancer activity [3]. SiO_2 and reduced graphene oxide (RGO) have indicated high potential for biomedical applications. SiO_2 and RGO can also be employed to adjust physicochemical properties of metal oxide nanoparticles such as ZnO. Graphene oxide and relevant materials like graphene/metal oxide nanocomposites have been more focused because of their low cost, easy obtainability and compatibility with different substrates [4]. Numerous studies have explored the cytotoxicity of graphene nanosheets in various types of cells since they were first offered as a potential biological application [5–7]. The cytotoxicity of graphene nanosheets is proportional to their size and concentration. Furthermore, aggregated graphene sheets may have a lower toxicity for nonadherent cells (red blood cells), while less packed graphene sheets have a higher toxicity for adherent cells (fibroblasts) [5].

Nourmohammadi et al. demonstrated visible light-driven photocatalytic activity of an electrophoretic deposition (EPD)-based GO/ZnO nanowire composite that inactivated Escherichia coli 99.5 percent when exposed to visible light for 1 h [8]. Their EPD approach allowed the positively charged GO sheets to penetrate into the nanowires and form a spider net-like structure, allowing for quicker photoexcited charge transfers and facilitating bacteria interaction with the

✉ Mahmoud Naseri
m.naseri@malayeru.ac.ir

✉ Saeideh Jafarinejad-Farsangi
s.jafarinejad@kmu.ac.ir

[1] Department of Physics, Faculty of Science, Malayer University, Malayer, Iran

[2] Student Research Committee, Kerman University of Medical Sciences, Kerman, Iran

[3] Physiology Research Center, Institute of Neuropharmacology, Kerman University of Medical Sciences, Kerman, Iran

[4] Department of Chemical Engineering, University of Toledo, Toledo, OH 43606, USA

Published online: 15 March 2022

sharp tips of the nanowires which results to physical damage to the bacteria's cell membrane. Another study confirmed Zn@GO's photocatalytic activity in the degradation of methylene blue (MB), a toxic compound prevalent in industrial effluents that is harmful to aquatic life [9]. ZnO@GO exhibited a 98.5 percent MB degradation efficiency under UV–visible light (15 min irradiation) compared to ZnO, which had a 49 percent MB degradation efficiency (60 min).

In the present study, a thermal treatment method was used to obtain zinc oxide nanocrystals from an aqueous solution containing polyvinyl pyrrolidone, zinc nitrates, and deionized water. Then the resulting nanocrystals were ground and calcinated. No other chemicals were added to the solution. Simplicity, a lack of by-product effluents, relatively low reaction temperatures, low cost, and an environmentally friendly alternative are among the advantages of this method.

2 Materials and methods

2.1 Preparation of the ZnO nanoparticles

Thermal treatment method has been successfully applied to prepare ZnO nanoparticles. To synthesize ZnO nanoparticles, an aqueous solution of PVP was made by dissolving 4 g of the polymer in 100 mL of deionized water at 80 °C. Then, 0.1 mmoL of zinc nitrate were added to the polymer solution and stirred for 2 h with a magnetic stirrer. The solution was heated in an oven at 100 °C for 24 h until the water evaporated. The remaining dried precursor was crushed and ground in a mortar to achieve a powder. Then, the powder was calcinated at 550 °C for 3 h to decompose any organic compounds and crystallize the ZnO nanoparticles.

2.2 Preparation of ZnO/SiO_2 and ZnO/SiO_2/RGO

In this step, 0.7 g of prepared ZnO nanoparticles were dispersed in 50 mL of ethanol and water solution by ultrasonic cleaning bath. After ultrasonic mixing for 30 min, 1.6 mL of ammonia solution and 8 mL of tetraethyl orthosilicate (TEOS) were added to zinc oxide in turn under vigorous stirring. The mixture was washed by ethanol and deionized water three times and finally dried at 60 °C for 12 h in an oven to prepare ZnO/SiO_2. Then, ZnO/SiO_2 was converted into ZnO/SiO_2/RGO nanocomposite by a simple polymerization method. After that, GO which was synthesized by graphite powder using modified Hummers method in previous work [5] was immersed in an aqueous solution containing CTAB and ultrasonicate. Next, ZnO/SiO_2 nanoparticles were added to the mentioned mixed solution while stirring to make a homogeneous dispersion and hydrazine hydrate was added to the suspension by stirring for 60 min. The suspension was centrifuged and washed by distilled water and ethanol. Finally, the resulting product was dried at 60 °C in vacuum for 24 h to make ZnO/SiO_2/RGO nanocomposite.

2.3 Cell culture

MCF-7, primary breast tumor cells KMBC/71 [6], and 3T3 normal fibroblasts were cultured in Dulbecco's Modified Eagle Medium (DMEM) supplemented with 10% FBS, and 1% penicillin/ streptomycin at 37 °C in an CO2 (5%) incubator.

2.4 MTT assay

The MTT assay is a well-established colorimetric method for measuring the viability of cells in cytotoxicity and proliferation studies. MCF-7, KMBC/71 and 3T3 fibroblasts cells were seeded separately in 96-well plates at a density of 8000 cells per well. After 24 h, they were exposed to different concentrations (250, 150, 62, 31, 15, 7, 3 μg mL^{-1}) of RGO, ZnO/SiO_2 and ZnO/SiO_2/RGO for 24 h. MTT (5 mg mL^{-1}) was added to each well and the cells were incubated at 37 °C for 4 h. Then, the medium was removed and 100 μL of dimethyl sulfoxide (DMSO) was added to each well. Finally, absorbance was measured at 570 nm by a microplate reader (BioTek ELX800, Winooski, Vermont, USA) and the viability of the cells were calculated according to the following equation: $\text{Cell Viability}(\%) = \frac{\text{ODSamples}}{\text{ODControl}} \times 100$.

3 Characterization

Through applying X-Ray Diffractometer (XRD, X'Pert PRO MPD, CuKα, $k = 0.15406$ nm), the crystalline structural phase of synthesized nanoparticles and nanocomposites was determined at room temperature and the microstructure of studied samples were investigated by field emission scanning electron microscope (FESEM) using JEOL JSM-6701 *F*-type instrument coupled with Energy dispersive X-ray (EDX) for elemental analysis. To evaluate the chemical interactions between RGO and magnetic ferrite nanoparticles, field emission scanning electron microscope, transform infrared spectroscopy (FTIR) spectra was recorded (PerkinElmer FTIR 1650 spectrometer). Raman spectroscopy measurements were taken using a Raman spectrophotometer Xplora PLUS with a 532 nm laser. By using a Micrometrics Belsorp mini system, Brunauer–Emmett–Teller (BET) surface area and pore-size distribution of samples were determined by the adsorption of nitrogen at 77 K.

4 Results and discussion

4.1 Structural and morphological analysis

Crystal structure and phase purity of ZnO/SiO_2, ZnO/SiO2/RGO nanocomposites and RGO nanosheets were analyzed by XRD technique. The main peaks of the XRD pattern of ZnO/SiO_2 nanocomposite are shown in Fig. 1. The characteristic peaks at $2\theta = 32.26°$, 34.91°, 36.48°, 47.88°, 56.95°, 63.36°, 66.79°, 68.36°, 69.45°, and 77.26° were observed from the XRD patterns of ZnO/SiO_2 nanocomposite, corresponding to the planes (100), (002), (101), (102), (110), (103), (200), (112), (201) and (202), respectively, indicating the existence of ZnO with hexagonal wurtzite phase (ICDD PDF: 79-0205) (indicated by star in Fig. 1). However, no amorphous pattern of vitreous silica or impurity was found. The XRD pattern of RGO showed the intense broad peak at 22.09° and a small peak at 43.16° corresponding to (002) and (102) planes, respectively (indicated by square in Fig. 1). The XRD result for GO presented in our previous research [10] show the appearance of sharp diffraction peak at $2\theta = 11.45°$, which is attributed to the (001) lattice plane corresponding to a *d* spacing of 7.72 angstrom. As a comparison, after the reduction process of GO, the diffractogram illustrates the disappearance of this strong peak and the appearance of a very broad (002) peak at $2\theta = 22.09°$, corresponding to a *d* spacing of 4.01 angstrom. The *d* spacing of RGO was reduced from 7.72 to 4.01 angstrom which proved that oxygen containing functional groups were removed efficiently, this suggests that the GO was reduced to rGO sheets during the reduction process because of the removal of the functional groups [11, 12]. The broad diffraction peak of RGO is close to the typical (002) diffraction peak of graphite (*d* spacing of around 3.3 angstrom at $2\theta \sim 26°$) [12–14]. These comparisons demonstrated that the crystalline structure can be restored after the reduction process used to synthesize few layer graphene [14]. It also revealed that the thin RGO nanosheet were stacked to each other to form thick piles structure due to the exist of strong Van der Waals' forces between each layer [15]. Another less intense peak can be seen at $2\theta = 43.16°$ with (102) orientation which attributed by the turbostratic band of disordered carbon materials [15–17]. The diffraction peaks of ZnO/SiO2/RGO nanocomposite were similar to those of hexagonal phase wurtzite ZnO nanoparticles (ICDD PDF: 5-0664); and the main peaks of ZnO/SiO2/RGO were seen in the XRD pattern of the ZnO/SiO_2 nanocomposite, Notably, a slightly broad peak around $2\theta = 20–30°$ (indicated by square in Fig. 1), which is seen in the patterns of RGO nanocomposites was assigned to the graphene nanosheet. Similar result has already been reported by Zafar et al. they stated that broad peak appears at $2\theta = 27.5°$ confirms the reduction of GO in a composite [18]. The RGO peaks in the nanocomposite suggested that the ZnO/SiO2/RGO nanocomposite was obtained successfully.

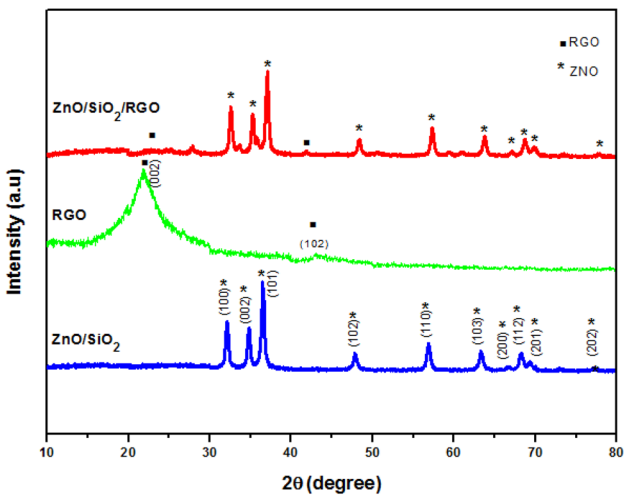

Fig. 1 XRD patterns of ZnO/SiO_2, RGO and ZnO/SiO_2/RGO

The average size of 55 and 64 nm was calculated for ZnO/SiO_2, ZnO/SiO2/RGO nanocomposites from the Debye Scherrer formula [7]. Figure 1

Figure 2 illustrates FESEM images and EDX analysis of ZnO/$SiO_2$and ZnO/SiO2/RGO nanocomposites. Figure 2a shows that ZnO/SiO_2 samples appear as quasi-spherical nanostructures and some ZnO/SiO_2 particles have been agglomerated. Figure 2b shows that the particles of ZnO/SiO_2 have been deposited on and between the RGO sheets. The average particle size of the ZnO/SiO_2 and ZnO/SiO2/RGO is ~43–47 nm. EDX spectrum of samples is shown in Fig. 2c and d. The names and percentages of the elements for the samples are shown in the labeling. The ZnO/SiO_2 nanocomposite is mainly composed of zinc, oxygen and Silicon (the order Zn > O > Si > C), and the presence of carbon is also detected, which is attributable to the presence of PVP surfactant in the nanoparticles [19]. While, for ZnO/SiO2/RGO nanocomposite the main constituent elements are carbon, Zinc and oxygen. That, the elemental composition percentage follows the order C > O > Zn > Si. From the inset table of Fig. 2c and d, it can be seen that the content of carbon in the ZnO/SiO2/RGO is higher than that of carbon in the ZnO/SiO_2 nanocomposite, which confirm the presence of RGO in the samples. Figure 2

Figure 3 indicates the FTIR spectra of ZnO/SiO_2, ZnO/SiO2/RGO nanocomposite samples. As seen in Fig. 3, the principal absorption band for Zn–O bond emerged at 469 cm^{-1} in the samples [20], which demonstrates the presence of zinc oxide in the sample. The absorption bands at 799, 1079 and 1639 cm^{-1} which represent terminal Si–OH deformation [21], asymmetric stretching

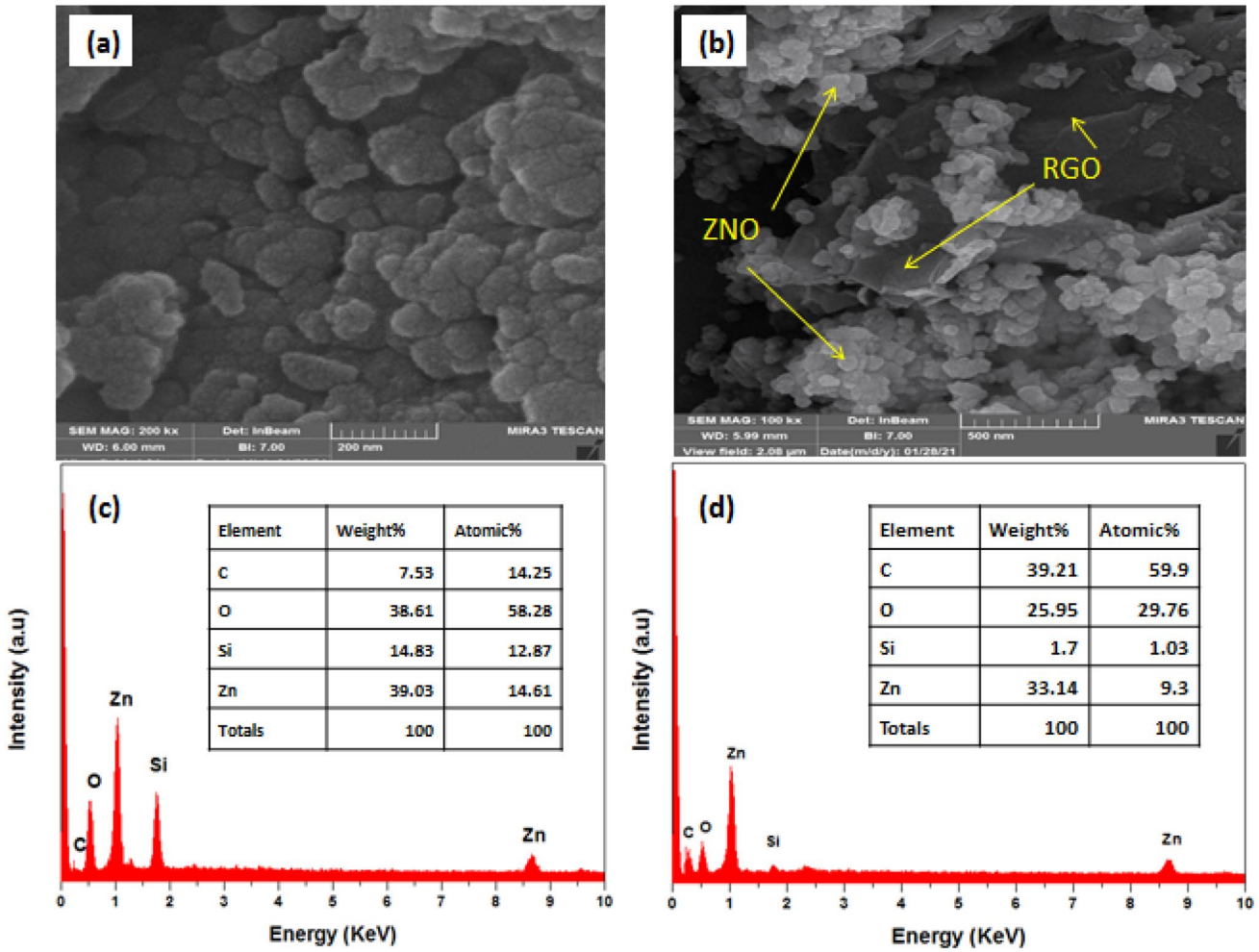

Fig. 2 FESEM images of **a** ZnO/SiO_2, **b** ZnO/SiO_2/RGO and EDX analysis of **c** ZnO/SiO_2, **d** ZnO/SiO_2/RGO

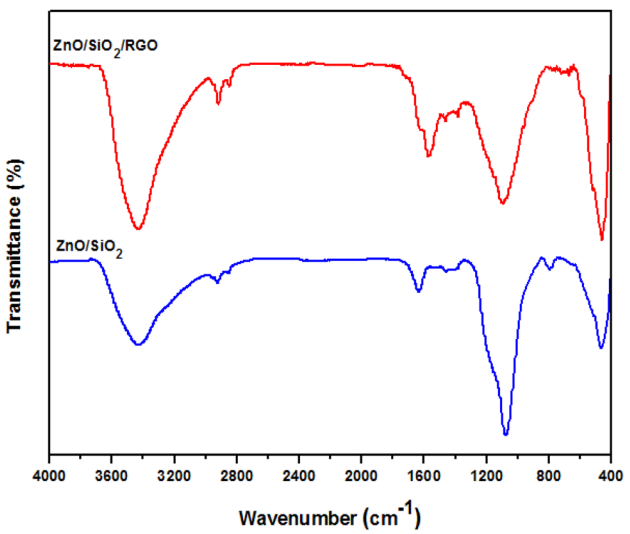

Fig. 3 FTIR spectra of ZnO/SiO_2 and ZnO/SiO_2/RGO

of Si–O–Si and the asymmetric and symmetric C=O are stretching for bonding related to the Zn–OH mode, respectively [20]. The peaks around 2924.24–2855.15 cm^{-1} can be attributed to the asymmetric and symmetric vibrations of C–H, respectively [22]. In the ZnO/SiO2/RGO sample, the appearance of new peaks around 600–1200 cm^{-1} can be associated with the Zn–C stretching bonding. Furthermore, the small peaks at ~1200–1800 cm^{-1} are associated with the presence of carboxyl and carbonyl groups in composite [23]. The broad peak at 3432 cm^{-1} in the FTIR spectrum of the both ZnO/SiO_2, ZnO/SiO2/RGO nanocomposite may be related to the O–H stretching vibration of the C–OH groups and water. Any shifts or changes in the position and intensity of peaks in the FTIR spectra of samples reveals the contribution of functional groups of GO with ZnO nanoparticles or partial reduction of graphene oxide [23]. Figure 3

The Raman spectra of ZnO/SiO_2, RGO and ZnO/SiO2/RGO are illustrated in Fig. 4. As shown in Fig. 4, several

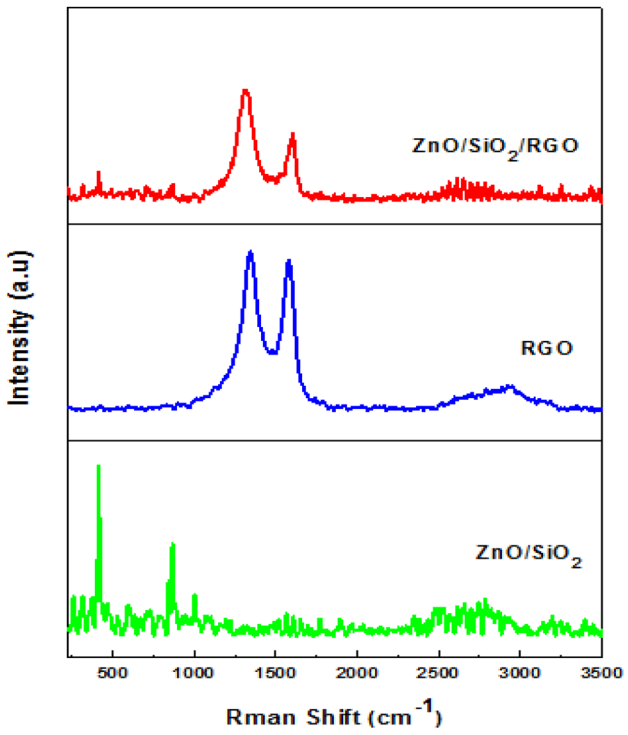

Fig. 4 Raman spectra of ZnO/SiO_2, RGO and ZnO/SiO_2/RGO

Raman peaks is observed in the ZnO/SiO_2 nanocomposite sample.

The prominently peaks at 313, 412, 866, and 1001 cm^{-1}, which correspond, A_1, E_{1TO}, A_1 and A_{1TO} modes, respectively. In addition, a sharp peak is observed around 412 cm^{-1}, originating from the hexagonal phase of ZnO [24, 25].The Raman spectra of RGO and ZnO/SiO2/RGO samples show the strong characteristic peaks located at 1344 and 1579 cm^{-1} corresponding to *D* and *G* bands, which are the typical graphene characteristic peaks [26]. That the *D* band arises due to A_{1g} symmetry and originates from the zone boundary phonons. This is attributed either to various defects of structure. However, the *G* band is first-order scattering, related to E_{2g} symmetry and corresponds to the Brillouin zone of crystalline sp^2 carbon structure [10].

Besides, a broad and shifted to higher wavenumber of 2*D* band were seen at 2952 cm^{-1} for RGO and RGO-nanocomposite. 2*D* band can be used to determine the layers of graphene as it is highly sensitive to stacking of graphene layers [26]. It is established that the *G* and 2*D* bands of single layer graphene sheets usually locate at 1585 and 2679 cm^{-1}, while for multi-layer graphene sheets (including 2–6 layers), the positions of the *G* and 2*D* bands shift into lower and higher wavenumbers, respectively [27, 28]. Furthermore, the 2*D*/*G* ratios of single, double, triple and multi (> 4)-layer graphene sheets are typically > 1.6, 0.8, 0.30 and 0.07, respectively [29, 30], previously Akhavan and coworkers [26] have reported single and bilayer GO sheets with 2*D*/*G* ratios in the range of 1.53–1.68 and 0.82–0.89, respectively. In our present work, the 2*D*/*G* ratios of the RGO sheets and RGO composite were calculated to have values between 0.15 and 0.21, suggesting the multilayer in present prepared graphene sheets. Furthermore, the *D*/*G* peak intensity ratio, known as a measure of the sp^2 domain size of graphene sheets containing sp^3 and sp^2 bonds. In our present work, the results indicate that the *D*/*G* ratio changes from 1.05 for RGO to 1.65 after the self-assembly in ZnO/SiO2/RGO composite, as seen in Fig. 4. The intensity ratios of *D* to *G* bands of the RGO and ZnO/SiO2/RGO samples are higher than that of GO, [15, 31] which can be attributed to the partial modification of surface oxygen containing functional groups. The Raman results indicated that the reduction of GO was successful. Figure 4

4.2 BET surface analysis

The surface areas of samples were obtained from nitrogen gas adsorption–desorption isotherms by Brunauer–Emmett–Teller (BET) analysis at 77 K. Figure 5 shows the BET surface area and relevant BJH pore size distribution (inset) of the ZnO/SiO2 and ZnO/SiO2/RGO nanocomposites. Based on Fig. 5, the type IV adsorption isotherms with hysteresis loops implied ZnO/SiO_2, ZnO/SiO2/RGO nanocomposite samples have mesopores. The existence of noticeable hysteresis loop in the isotherm is ascribed to the presence of mesopore among nanocomposite samples. The average pore diameter of both the samples were discovered to be 20.6 nm (for ZnO/SiO_2) and 30.5 nm (for ZnO/SiO2/RGO), and specific surface areas of ZnO/SiO_2 and ZnO/SiO2/RGO nanocomposites were 6.9 and 16.7 $m^2\ g^{-1}$, respectively. However, the specific surface area of ZnO/SiO2/RGO was higher than that of ZnO/SiO_2 nanoparticles. Because the ZnO/SiO_2 nanoparticles can unfold on the RGO sheets, the larger specific surface and distribution of nanoparticles in ZnO/SiO2/RGO nanocomposites can provide more adsorption and reaction sites, which indicates that the generation of pore can enlarge the surface area activity (Fig. 5) [32].

4.3 Cell viability

As shown in Fig. 6, RGO had no significant toxicity in breast tumor (MCF-7 and BCT71) and 3T3-fibroblast cells. Instead, the viability of breast tumor cells reduced after exposure to ZnO/SiO_2 and ZnO/SiO2/RGO at concentrations above 7 µg mL^{-1}. The cytotoxicity of ZnO/SiO_2 and ZnO/SiO2/RGO in 3T3-fibroblasts was significant at concentrations above 31 and 15 µg mL^{-1}, respectively. According to the results, it seems that cytotoxicity ZnO/SiO_2 and ZnO/SiO2/RGO in normal fibroblasts were less than their cytotoxicity

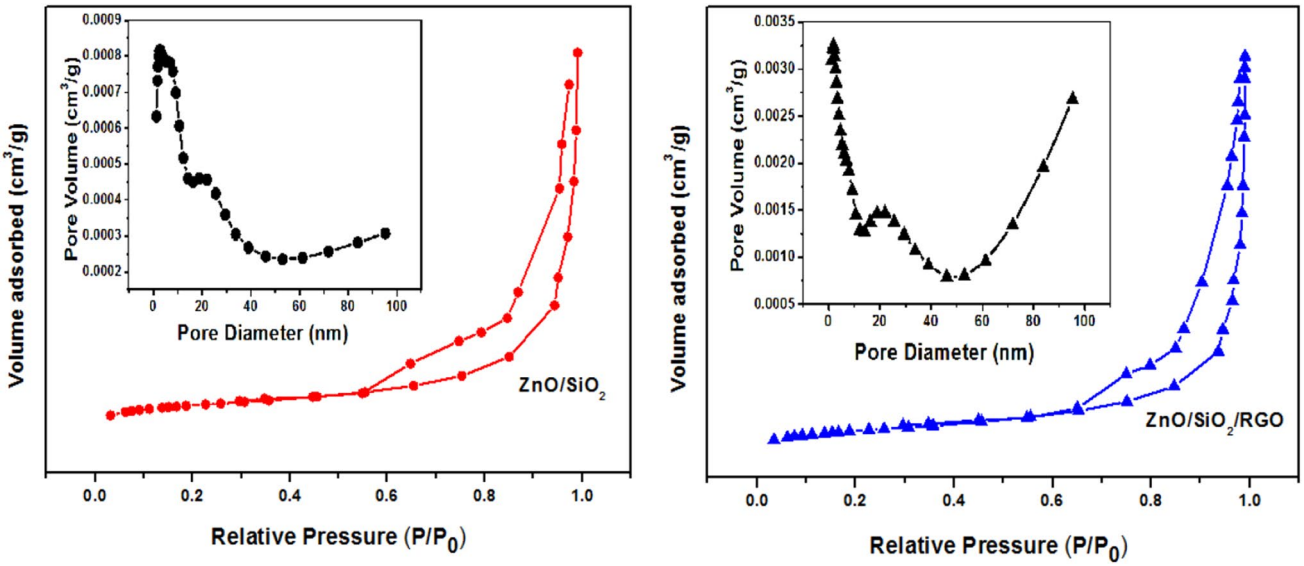

Fig. 5 Nitrogen adsorption–desorption isotherms, and (inset) corresponding pore size distribution of ZnO/SiO_2 and ZnO/SiO2/RGO

in breast tumor cells. Interestingly, the fibroblasts population increased at concentrations below 15 μg mL^{-1}. Ahamed et al. showed that SnO_2–ZnO/RGO nanoparticles were more biocompatible toward normal cells than SnO_2–ZnO and ZnO nanoparticles alone [33]. Although RGO has a lower cytotoxic effect on fibroblasts and breast tumor cells than ZnO/SiO_2 and ZnO/SiO_2/RGO, its biocompatibility has not been fully established. Alive cells exposed to graphene oxide have been shown to have further negative consequences, such as changes in gene expression in tumor cells [5] or chromosomal abnormalities in stem cells [5], which alter cell fate and render them sensitive or resistant to treatments. However, the cytotoxicity of ZnO/SiO_2 and ZnO/SiO2/RGO may be due to Zn ion. There are several studies that reports the Zn^{2+} related cytotoxicity of ZnO nanoparticles [34–38]. It seems that the acidic pH of the tumor environment facilitates Zn^{2+} release from ZnO which in return promotes more cell death in tumor cells in compare to the normal cell [37]. Furthermore, uptake of ZnO nanoparticles by phagocytes and subsequent release of Zn ion in the acidic pH in the phagosomes results in progressive severe lung injuries [34]. According to Shen et al. study, intracellular released Zn^{2+} increased reactive oxygen species, transition metal ions and protein activity disequilibrium which leads to cytotoxicity [39]. Figure 6

5 Conclusions

In summary, ZnO nanoparticles were fabricated by thermal treatment method and ZnO/SiO_2 and ZnO/SiO2/RGO nanocomposites were obtained using polymerization method. The XRD patterns revealed hexagonal quartzite structure of samples. The FESEM images showed that the graphene nanosheets were decorated with ZnO/SiO_2 nanocomposite. Furthermore, ZnO/SiO_2 and ZnO/SiO2/RGO seem to be more biocompatible for normal cells compared with tumor cells, which is considered as an advantage in medical application. However, further investigations are needed to explore biocompatibility of these nanoparticles in more details.

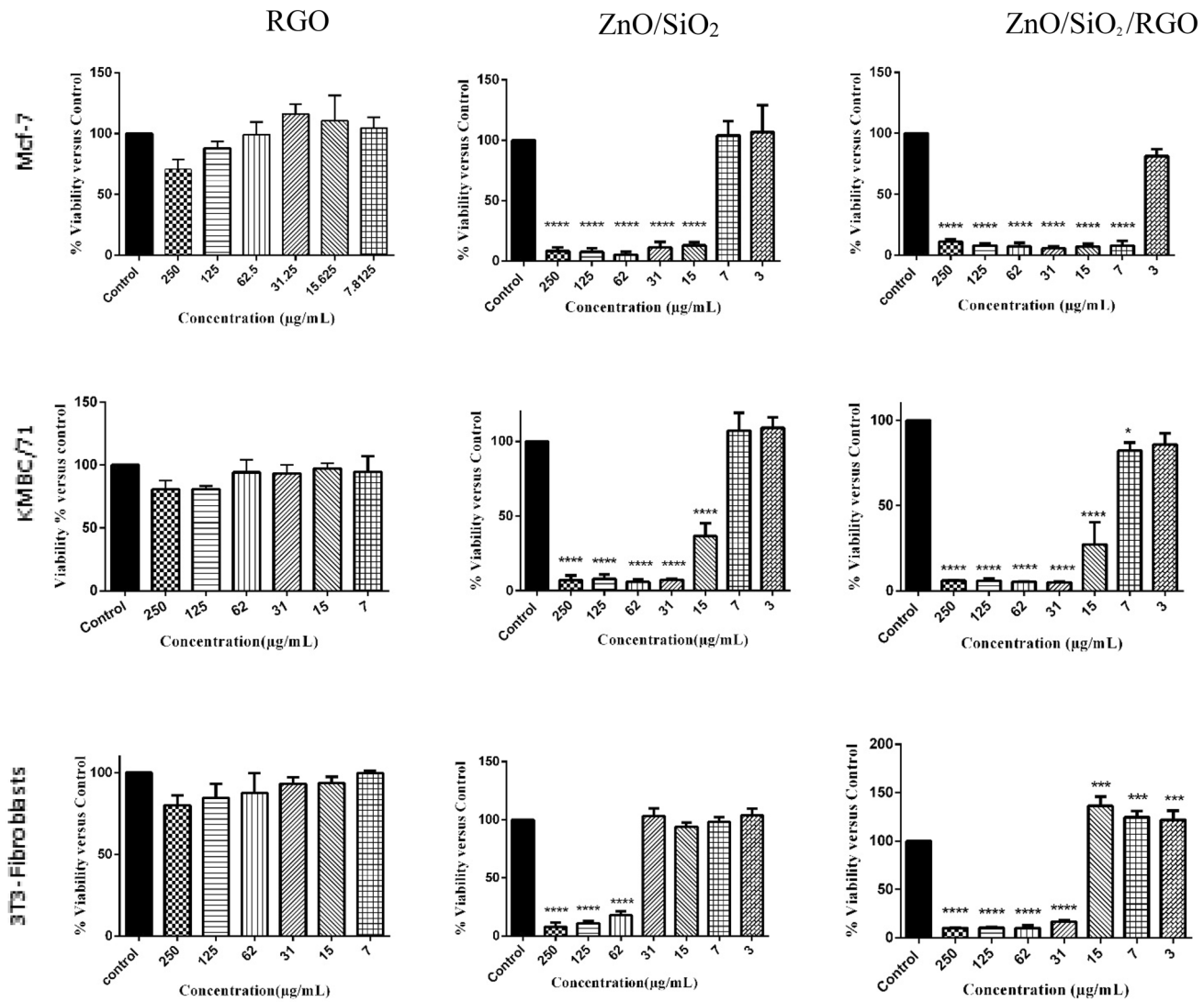

Fig. 6 Fig. 5. Cell viability, The effects of RGO, ZnO/SiO_2 and ZnO/SiO_2/RGO on the viability of MCF-7, KMBC/71 and 3T3-fibroblast cells. $n=6$; $^{*}P<0.05$, $^{**}P<0.001$, $^{***}P<0.001$, $P<0.0001$

Acknowledgements This work was supported by the Ministry of Science, Research and Technology, Malayer University of Iran and generously supported by grants from the Deputy of Research of Kerman University of Medical Sciences Medical Sciences (KUM) under Grant No. 98000936. All procedures performed in studies involving human participants were in accordance with the ethical standards of Kerman University of Medical Sciences (KMU) Ethics committee IR.KMU.REC.1398.025)

Declarations

Conflict of interest The authors did not receive support from any organization for the submitted work.

References

1. M. Ahamed, M.J. Akhtar, M.M. Khan, H.A. Alhadlaq, Colloids Surf. B. Biointerface. **172**, 152 (2018)
2. S.K. Verma, P.K. Panda, E. Jha, M. Suar, S.K. Parashar, Sci. Rep. **7**, 1 (2017)
3. P.K. Mishra, H. Mishra, A. Ekielski, S. Talegaonkar, B. Vaidya, Drug Discov. Today **22**, 1825 (2017)
4. K.A. Wanderley, A.M. Leite, G. Cardoso, A.M. Medeiros, C.L. Matos, R.C. Dutra, P.A. Suarez, Braz. J. Chem. Eng. **36**, 1165 (2019)
5. K.H. Liao, Y.S. Lin, C.W. Macosko, C.L. Haynes, ACS Appl. Mater. Interfaces. **3**, 2607 (2011)
6. O. Akhavan, E. Ghaderi, A. Akhavan, Biomaterials **33**, 8017 (2012)
7. M.S. Hashemi, S. Gharbi, S. Jafarinejad-Farsangi, Z. Ansari-Asl, A.S. Dezfuli, Toxicol. Vitro. **65**, 104796 (2020)
8. A. Nourmohammadi, R. Rahighi, O. Akhavan, A. Moshfegh, J. Alloy. Compd. **612**, 380 (2014)

9. R. Atchudan, T.N.J.I. Edison, S. Perumal, D. Karthikeyan, Y.R. Lee, J. Photochem. Photobiol. B **162**, 500 (2016)
10. M. Chireh, M. Naseri, S. Ghiasvand, J. Photochem, Photobiol **385**, 112063 (2019)
11. M. Sookhakian, Y.M. Amin, R. Zakaria, S. Baradaran, M.R. Mahmoudian, M. Rezayi, W.J. Basirun, Ind. Eng. Chem. Res. **53**, 14301 (2014)
12. A. Alazmi, S. Rasul, S.P. Patole, P.M. Costa, Polyhedron **116**, 153 (2016)
13. J. Li, X. Liu, J. Sun, Ceram. Int. **42**, 2085 (2016)
14. X. Jiao, Y. Qiu, L. Zhang, X. Zhang, RSC Adv. **7**, 52337 (2017)
15. N.M.S. Hidayah, W.W. Liu, C.W. Lai, N.Z. Noriman, C.S. Khe, U. Hashim, U.C. Lee, in AIP conference proceedings, **1,** p. 150002 2017
16. B. Gupta, N. Kumar, K. Panda, V. Kanan, S. Joshi, I. Visoly-Fisher, Sci. Rep. **7**, 1 (2017)
17. M.A. Faiz, C.C. Azurahanim, S.A. Raba'ah, M.Z. Ruzniza, Result. Phys. **16**, 102954 (2020)
18. Z.K. Ghouri, M. Motlak, S. Afaq, N.A. Barakat, A. Abdala, Nanotechnol. Rev. **8**, 661 (2019)
19. M. Chireh, M. Naseri, H. Ghaedamini, Adv. Powder Technol. **32**, 4697 (2021)
20. M.B. Mohamed, M.H. Abdel-Kader, A.A. Alhazime, Int. J. Appl. Ceram. Technol. **16**, 1209 (2019)
21. B.A. Al-Asbahi, Mater. Res. Bull. **89**, 286 (2017)
22. Z. Durmus, B.Z. Kurt, A. Durmus, Chem. Sel. **4**, 271 (2019)
23. S. Alamdari, M.S. Ghamsari, H. Afarideh, A. Mohammadi, S. Geranmayeh, M.J. Tafreshi, M.H. Ehsani, Opt. Mater. **92**, 243 (2019)
24. S. Abdolhosseinzadeh, H. Asgharzadeh, S. Sadighikia, A. Khataee, Res. Chem. Intermed. **42**, 4479 (2016)
25. A.M. Ali, A.A. Ismail, R. Najmy, A. Al-Hajry, J. Photochem. Photobiol. A **275**, 37 (2014)
26. O. Akhavan, Carbon **81**, 158 (2015)
27. I. Calizo, A.A. Balandin, W. Bao, F. Miao, C.N. Lau, Nano Lett. **7**, 2645 (2007)
28. K.N. Kudin, Nano Lett. **8**, 36 (2008)
29. T. Balashov, A.F. Takcs, W. Wulfhekel, J. Kirschner, Phys. Rev. Lett. **97**, 187201 (2006)
30. K.S. Kim, Nature **457**, 706 (2009)
31. W. Guo, B. Zhao, Q. Zhou, Y. He, Z. Wang, N. Radacsi, ACS Omega **4**, 10252 (2019)
32. Y. Lin, J. Dong, J. Dai, J. Wang, H. Yang, H. Zong, Inorg. Chem. **56**, 14960 (2017)
33. M. Ahamed, M.J. Akhtar, M.M. Khan, H.A. Alhadlaq, Int. J. Nanomed. **16**, 89 (2021)
34. W.S. Cho, R. Duffin, S.E. Howie, C.J. Scotton, W.A. Wallace, W. MacNee, K. Donaldson, Part. Fibre Toxicol. **8**, 1 (2011)
35. S. Tada-Oikawa, G. Ichihara, Y. Suzuki, K. Izuoka, W. Wu, Y. Yamada, S. Ichihara, Toxicol. Rep. **2**, 692 (2015)
36. D. Cao, X. Shu, D. Zhu, S. Liang, M. Hasan, S. Gong, Nano Converg. **7**, 1 (2020)
37. K.H. Muller, J. Kulkarni, M. Motskin, A. Goode, P. Winship, J.N. Skepper, A.E. Porter, ACS Nano **4**, 6767 (2010)
38. B. Wu, J. Wu, S. Liu, Z. Shen, L. Chen, X.X. Zhang, H.Q. Ren, Environ. Sci. Nano **6**, 635 (2019)
39. C. Shen, S.A. James, M.D. de Jonge, T.W. Turney, P.F. Wright, B.N. Feltis, Toxicol. Sci. **136**, 120 (2013)